frontiers | Frontiers in Energy Research

TYPE Review
PUBLISHED 02 December 2024
DOI 10.3389/fenrg.2024.1463024

OPEN ACCESS

EDITED BY
Kaiwen Sun,
University of New South Wales, Australia

REVIEWED BY
Yuanhang Cheng,
Nanjing University of Science and Technology, China
Diksha Thakur,
National Central University, Taiwan

*CORRESPONDENCE
Dawen Li,
dawenl@eng.ua.edu

RECEIVED 11 July 2024
ACCEPTED 04 October 2024
PUBLISHED 02 December 2024

CITATION
Brown M and Li D (2024) Interfacial engineering for high performance carbon-based perovskite solar cells.
Front. Energy Res. 12:1463024.
doi: 10.3389/fenrg.2024.1463024

Interfacial engineering for high performance carbon-based perovskite solar cells

Megan Brown and Dawen Li*

Department of Electrical and Computer Engineering, The University of Alabama, Tuscaloosa, AL, United States

Perovskite solar cells fabricated with carbon-based counter electrodes demonstrate decreased cost, enhanced simplicity and speed of production, and increased stability compared to those produced with standard metallic electrodes. This significant improvement of device stability, cost reduction, and production scalability indicates a promising direction for commercial development and availability of perovskite solar technology. The main limitation of carbon-based perovskite devices is the flawed contact between the carbon electrode and perovskite film which decreases device quality and performance, thereby necessitating treatment of the carbon/perovskite interface. This review provides an overview of the current state of carbon-based perovskite devices, discusses progress in carbon/perovskite interface modification methods, and suggests future directions for the research of carbon electrode/perovskite film interface manipulation.

KEYWORDS

perovskite solar cells, carbon contact, interfacial engineering, C-PSCs, defects passivation, stability

1 Introduction

Perovskite solar cells (PSCs) have developed rapidly since 2009, when the material was first investigated for use in photovoltaic devices as a light absorption layer. Due to the halide composition of perovskite material, perovskite precursor is cheap, easy to produce, and has a versatile and bandgap tunable crystal structure (Cheng and Lin, 2022). Perovskite materials can be produced in a wide variety of organic, inorganic, and hybrid makeups (Li et al., 2022; Zhang et al., 2023; Ling et al., 2019). As of 2024 PSCs have reached photoelectric conversion efficiency (PCE) values of over 26%, which is comparable to the PCE of silicon-based solar cells. However, the technology struggles with long-term device stability and is especially vulnerable to perovskite degradation due to moisture and increased temperature during operation (Bogachuk et al., 2020; Bidikoudi and Stathatos, 2023; Wu et al., 2019; NREL; Wang R. et al., 2019; Grancini et al., 2017).

PSC structures typically contain the layers of conductive glass substrate, electron transport layer (ETL), perovskite absorber, hole transport layer (HTL), and metallic electrode. These layers can be configured to form negative-intrinsic-positive regular (n-i-p) structures and positive-intrinsic-negative/inverted (p-i-n) architectures that are additionally categorized as planar or mesoscopic depending on the inclusion of an extra mesoporous layer. The low crystallization energy of perovskite precursor allows perovskite film to be fabricated by solution processing at room temperature, which establishes the potential for cost-effective large-scale production of perovskite solar cells (McMeekin et al., 2019). However, the metallic electrode layer of PSCs—which is usually composed of gold or

silver—introduces high material costs and additional time and energy consumption to the fabrication process through the necessity of vacuum deposition (Gan et al., 2023). Atom/ion migration and corrosion of the metallic electrode also decrease the stability of PSCs. As such, an alternative for metallic electrodes has been found in carbon electrodes (CEs). CEs are low cost, can be fabricated with simple processes in ambient conditions, and have a chemically stable nature and hydrophobic properties that can improve the stability of PSCs. The switch to utilization of CEs introduces vast improvements to the primary issues of PSC commercialization: long-term device stability and scalable production (Baranwal et al., 2016). This review aims to discuss the current state-of-the-art carbon-based PSCs (C-PSCs) and recent developments related to the technology's main issue: poor contact between the carbon electrode and perovskite light absorption layer. Interfacial engineering shows great potential as a method for improving C-PSC performance and long-term stability (Dong et al., 2021; Ye et al., 2019). Pertinent background information related to this technology includes the strengths and weaknesses of C-PSCs, typical device structure, and the material compositions of carbon electrodes (Section 2). This comprehensive discussion of interfacial engineering for the improvement of C-PSC performance will examine methods including the addition of buffer layers and layer treatments (Section 3), CE doping and CE solvent choice (Section 4), perovskite crystallization control (Section 5), and the impact of these methods on perovskite solar module (PSM) production (Section 6).

2 Background

2.1 Benefits and limitations of carbon-based perovskite solar cells (C-PSCs)

The use of carbon counter electrodes for PSCs has the primary benefit of increased device stability compared to reference metal-based PSCs. This is due to the hydrophobic properties, thermal stability, and chemical inertness of the carbon material, as well as that carbon does not exhibit the atom/ion migration and corrosion that affects PSCs with metallic electrodes (Wang et al., 2020; Qiu et al., 2019; Fagiolari and Bella, 2019; Zhao et al., 2024). Degradation due to moisture is a significant source of instability for perovskite materials, making the hydrophobicity of carbon an essential factor of C-PSC stability improvement (Boyd et al., 2019; Calabrò et al., 2020). Carbon is less expensive than the materials that make up metallic electrodes—most often the precious metals gold and silver—but has a work function value close to that of gold (Zouhair et al., 2024). In addition, carbon electrodes can be fabricated through solution processing in ambient conditions, making the production process more simple and cost-effective than the vacuum deposition which is necessary for metallic electrode formation (Beynon et al., 2023; Zhu et al., 2021; Tountas et al., 2023). In particular, C-PSCs can be produced without a hole transport layer (HTL), reducing fabrication costs and complexity and eliminating a source of recombination loss of charged carriers within the device (Sulistianto et al., 2024). These factors increase the commercialization and large-scale production viability of carbon-based devices compared to metal-based PSCs (Yu et al., 2023). CEs can also be utilized in the fabrication of flexible PSCs (Peng et al., 2021). Current C-PSCs have lower PCE values than reference metal-based devices, which is attributed to multiple factors including the lower conductivity of carbon electrodes versus metallic electrodes, poor contact between the carbon electrode and perovskite film layer (causing voltage loss), and unfavorable mismatch between the CE and perovskite film energy levels (Nazir et al., 2022; Chen and Yang, 2019; He et al., 2019; Zhang et al., 2020). Currently, the highest certified PCE value for C-PSCs is 21.9% (Wang Y. D. et al., 2022; Aji et al., 2024).

2.2 C-PSC device structure

Nowadays, C-PSCs are typically fabricated at low-temperature conditions (LT) with planar architectures. Since this review focuses on the current state-of-the-art C-PSCs, the historical development, including obsolete high-temperature processing and complex mesoscopic architectures, can be found in the referenced review articles (Bogachuk et al., 2020; Bidikoudi and Stathatos, 2023; González et al., 2022). Due to the similarity to metallic electrode device structures, previously explored perovskite device modifications such as crystallization control techniques and passivation methods can be applied to C-PSCs. In contrast with standard PSCs, HTL inclusion is optional in C-PSC fabrication (Maniarasu et al., 2018; Chen and Yang, 2017). Due to poor contact and high rates of recombination at the carbon electrode/HTL interface, many C-PSCs are fabricated without a HTL (González et al., 2022). As such, carrier extraction efficiency is an important metric for device performance in HTL free C-PSCs and is affected by the quality at the perovskite/carbon contact (Chen et al., 2019). The exclusion of HTLs can also decrease production cost and complexity, facilitating commercial scalability (Zhang et al., 2019). However, the addition of modified HTLs into C-PSC structure can improve device performance and has been explored in cases with resulting improvement to the carbon/perovskite interface quality, PCE, or device stability (Aung et al., 2022).

2.3 Carbon electrode composition

The material characteristics of the type of carbon selected for a CE have a significant impact on the performance of C-PSCs. The most common carbon compositions utilized in C-PSCs include graphite, graphene, carbon black, carbon nanotubes, and composites of these carbon allotropes (Pandey et al., 2023). Factors affecting the conductivity of the CE include the carbon particle size, the interconnection of the particles, and the film thickness.

Graphite is a common, inexpensive allotrope of carbon and has multiple variants with beneficial characteristics. The size of graphite particles is related to improved CE/perovskite layer contact and hole collection efficiency, with smaller particle sizes having a larger area of surface contact and increased contact quality. The microcrystal height of graphite flakes is indirectly related to the sheet resistance of the resulting CE. Porous graphite is highly hydrophobic, which improves PSC stability, and ultra-thin graphite has increased surface area without a change in the material conductivity, which results in

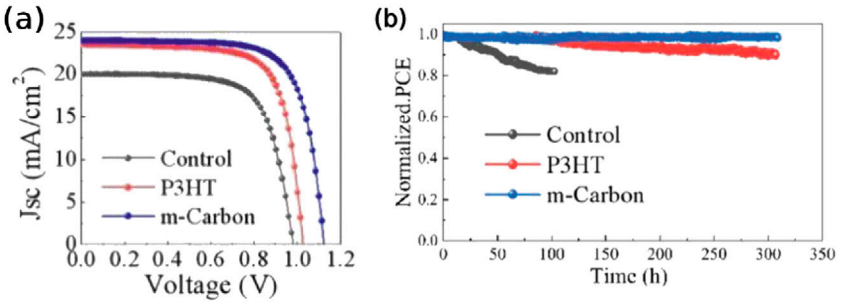

FIGURE 1
(A) C-PSC current density vs. voltage curves for devices with different device configurations. **(B)** Unencapsulated cell operational stability in ambient air and with maximum power point tracking (Lu et al., 2023).

improved contact and hole collection. Nevertheless, graphite CEs have a relatively high defect density compared with metallic electrodes. Graphene is a single layer of honeycomb-structured carbon atoms with high conductivity and strength. These characteristics, along with the transparency of graphene sheets, make graphene CEs well suited for flexible applications. Carbon black (CB) has a hexagonal sheet structure consisting of aggregate carbon particles. CB has a relatively low resistivity and nano-CB has reduced pore space, which improves the conductivity, CE/perovskite contact, and hole extraction capabilities. Carbon nanotubes (CNTs) are hollow cylinders made from sheets of graphene that exhibit high conductivity, strength, and flexibility (Zhang et al., 2024a). They are also transparent and can be used in flexible and bifacial PSCs, but are vulnerable to oxidation and corrosion. The incorporation of CNTs into perovskite material has resulted in passivation effects and improved charge mobility (Lin et al., 2020).

Composite CEs are created from multiple types of carbon with the goals of the resulting CE having high conductivity, ease of processing, and low cost. Common composite CE compositions include CB mixed with graphite or graphene. For a comprehensive discussion of carbon allotropes for CE applications please refer to Reference (Meng et al., 2024). A variety of fabrication methods can be utilized to produce CEs for photovoltaic applications. Methods such as blade/doctor coating, screen printing, inkjet printing, and slot-die coating are often chosen for their low costs, scalability, adaptability, and compatibility with low-temperature production environments. The composition of the CE and its compatibility with the perovskite film is one of the factors that determines the interface quality between device layers (Yue et al., 2016).

3 Carbon electrode/perovskite layer interface manipulation

As discussed, poor contact between the CE and perovskite film layer is one of the primary obstacles to be overcome to improve the PCE of C-PSCs (Zhang et al., 2018; Meng et al., 2019; Chu et al., 2020). Interface contact quality is also a determining factor of long-term device stability (Xiao et al., 2017; Niu et al., 2016). To this end, the CE/perovskite interface can be modified for possible improvement via enhancing the compatibility between the two layers. The properties that can be enhanced include CE layer conductivity, charge transfer and extraction, material morphology, defect density, and moisture resistance. CE/perovskite contact quality also significantly impacts charge recombination at interfaces (Qiu and Yang, 2020). In general, interface modification techniques involve manipulating the carbon material, the perovskite film, or both, as well as the addition of a distinct interfacial layer. Section 3 of this review focuses on strategies for the addition of interfacial buffer layers.

The addition of a buffer layer at the CE/perovskite film interface is a common method used to improve the interface contact and overall device performance and stability, though the inclusion of a buffer layer can add additional fabrication steps and costs to C-PSC production. The interfacial layer typically passivates surface defects to reduce nonradiative recombination and serves as a bridge to facilitate charge transport and collection by establishing a favorable energy level alignment. Lu et al. (2023) added a polythiophene (P3HT) layer in between the NiOx HTL and perovskite film, resulting in a PCE of 20.8% with high stability. The device followed a structure of ITO/SnO_2/$MAPbI_3$/P3HT/NiOx/CE, including a blade coated carbon black and graphite powder electrode. This CE was modified (m-Carbon) and consisted of a diluted carbon layer followed by an undiluted layer to facilitate charge collection. The P3HT buffer layer reduced charged carrier recombination loss, prevented corrosion of the perovskite absorber from the CE, and inhibited moisture infiltration. The inorganic/organic NiOx and P3HT composite HTL is a dense and pin-hole free film, working together to minimize degradation of the perovskite film. The performance enhancement is also partially ascribed to the improved alignment between the $MAPbI_3$ perovskite and NiOx energy levels with addition of P3HT buffer layer. The incorporation of the P3HT buffer layer, along with modified carbon electrode, increased the PCE to 20.8% as compared to the 13.4% from the reference devices with NiOx HTL only, as shown in Figure 1A. As the P3HT layer also enhanced the hydrophobicity of the underlying perovskite film, the champion device retained over 80% efficiency after 300 h in ambient air at 40%–50% relative humidity and at its maximum power point, as shown in Figure 1B. The optimal thickness for the P3HT layer was found to be approximately 25 nm.

The same group, Li Y. Q. et al. (2023) achieved a device with 20.14% PCE with a PSC structure of ITO/SnO_2/$FA_{0.6}$ $MA_{0.4}PbI_3$ perovskite/P3HT/CTAB-doped NiOx (m-NiOx)/CE by adding alkyl ammonium bromide (CTAB) to the NiOx layer. The device included

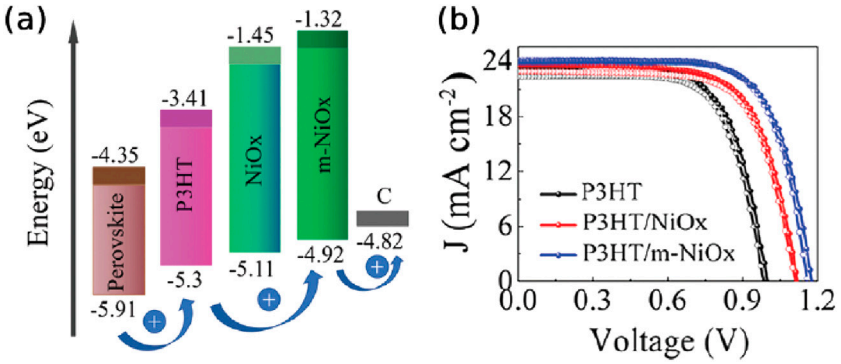

FIGURE 2
(A) Energy level diagram of device materials. **(B)** Current density vs. voltage curves for devices with various HTLs © 2023 Wiley-VCH GmbH (Li Y. Q. et al., 2023).

a blade coated CE and a $FA_{0.6}MA_{0.4}PbI_3$ perovskite composition and developed ohmic contact at the CTAB-doped NiOx/CE interface. The CTAB-doping modified the NiOx work function to facilitate hole transport at the P3HT/m-NiOx interface and collection at the CE contact as shown in Figure 2A. Compared to those PSCs with P3HT and composite P3HT/NiOx HTLs, the PSCs with P3HT/ modified NiOx composite HTLs demonstrated enhanced PCE, as shown in Figure 2B. The bilayer HTL again demonstrated reduced degradation of the perovskite layer from the CE solvents during fabrication. Compared to the PSCs with P3HT HTLs only, which retained 80% of the initial PCE after 150 h, the PSCs with composite P3HT/m-NiOx HTLs demonstrated a stability of 95% efficiency retained after 275 h when measured at maximum power point.

Interface manipulation at multiple layer boundaries can also be applied to improve the favorable properties of C-PSC devices. Li S. Q. et al. (2023) fabricated a HTL free device with dual interface modification, applying FABr to the bottom of the perovskite absorber and FAI to the top of the perovskite layer. The ITO/ SnO_2/FABr/$MAPbI_3$/FAI/CE structured device was fabricated in ambient air conditions and included a blade coated CE consisting of a commercial carbon paste. The FAI solution was deposited on top of the CE and was allowed to stand on the surface prior to annealing, filling in gaps between the CE and perovskite layers. This interface manipulation resulted in increased CE/perovskite layer contact quality, perovskite crystallinity, and hydrophobicity for the device. The underlying FABr layer was used to regulate the composition at the bottom region of the MAPbI3 perovskite films and enhance the SnO_2/perovskite interface quality. The inclusion of dual interface modifications also reduced the interface defect density and resulted in a favorable energy level alignment. The champion device had a PCE of 17.49% in air and a stability of 96% efficiency retained after 1,440 h in ambient air conditions. A vast improvement in stability performance resulted from both bottom interface modification (BIM) only and dual interface modification (DIM).

Zou et al. (2023) added a mixture of zinc phthalo cyanine (ZnPc) and $CsPbBr_3$ quantum dots on the top of the $CsPbBr_3$ perovskite as an interfacial layer, resulting in a passivation effect, improved layer contact, and optimized energy alignment at the CE/perovskite interface. Although the PCE was just above 10%, the device exhibited decreased surface roughness and unencapsulated stability of 99.5% efficiency retained after 6 months (or approx. 4,380 h) in ambient air at approx. 30% relative humidity. The improved performance with the ZnPc mixed CsPbBr3 QDs modification layer was attributed to passivation of interface trap states and optimized energy level alignment, enhancing carrier extraction and reducing non-radiative charged carrier recombination. Though the device PCE is less than 50% of the current highest C-PSC PCE, the extended ambient air stability of this device is highly promising for the long-term stability necessary for C-PSC commercialization—demonstrating the significance of interfacial buffer layers in the advancement of C-PSC technology.

Zhang et al. (2024b) utilized a surface passivating agent, potassium laurate (KLA), for effective dual-active-site passivation in a ITO/SnO_2/$FAMAPbI_3$/KLA/CE structured device. The KLA passivator with both carboxylate groups and K+ cations synergistically passivated uncoordinated Pb^{2+} and I^- anionic defects, thereby suppressing non-radiative charged carrier recombination at the perovskite/CE interface. The KLA materials within the perovskite film at optimal concentrations also improved the morphology of the perovskite film and increased the perovskite grain size. In addition, the KLA treated device showed improved energy level alignment between the perovskite film and both the SnO_2 ETL and CE. The champion device resulted in a reduction of hysteresis, a PCE of 16.10%, and retained 85% of its initial PCE after 1,440 h of storage in an ambient air environment at 20°C–25°C and 50%–60% relative humidity. In comparison, the reference device retained only 64% of its initial PCE under the same duration and conditions.

Tang et al. (2024) utilized various alkylammonium chlorides—including butylammonium chloride (BACl), octylammonium chloride (OACl), and decylammonium chloride (DACl)—as passivating interface layers within their HTL free ITO/ SnO_2/$FAMAPbI_3$/CE structured devices. These alkylammonium chlorides were used to form 2D perovskite structures at the 3D perovskite boundary as shown in Figure 3A. The surface passivation with alkylammonium chlorides resulted in improved uniformity of perovskite grain sizes, reduced defects at grain boundaries, and created favorable energy level alignment between the perovskite film and the composite carbon black/graphite flake CE. The DACl device

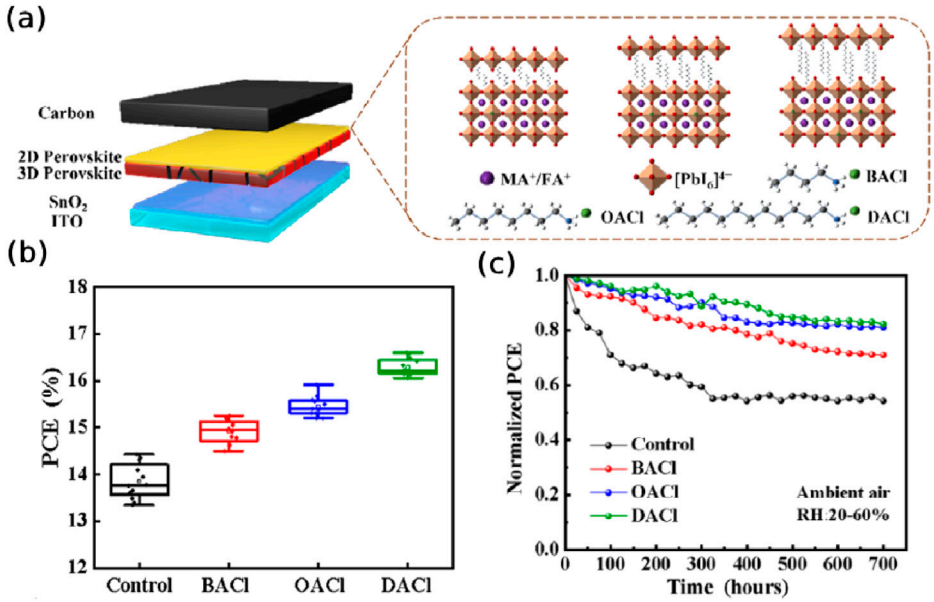

FIGURE 3
(A) Device structure diagram. **(B)** PCE comparison for various passivating interface layers. **(C)** Ambient air storage stability test for alkylammonium chloride passivated devices © 2023 Wiley-VCH GmbH (Tang et al., 2024).

showed the best performance, demonstrating reduced nonradiative recombination, the lowest defect density, and a PCE of 16.56% compared to the reference's 14.43% (Figure 3B). The devices underwent multiple stability tests, including 700 h of ambient storage at approximately 20°C and 20%–60% relative humidity where the OACl and DACl devices retained over 80% of their initial PCEs to the reference device's over 55% as seen in Figure 3C.

Interface engineering at interfaces other than the CE/perovskite film contact also exhibits significant improvements in C-PSC performance and stability. Wang H. L. et al. (2024) demonstrated improved perovskite crystal size and film morphology, efficient carrier extraction, and passivation of defect states through the inclusion of a thin naphthaleneimide derivative (CATNI) based interfacial layer between the perovskite layer and SnO_2 ETL. The fabricated PSC device was fully printed, utilizing a 2D $FA_{0.4}MA_{0.6}PbI_3$ perovskite and resulting in a 18.9% PCE, which is primarily attributed to the enhanced open-circuit voltage (Voc). This PSC had a stability of 95.5% after 1,000 h in dark conditions at 30% relative humidity and 25°C where the reference device retained only 88% efficiency. In another stability test the CATNI modified device retained 44% efficiency after 300 h under continuous 1 sun illumination *versus* the reference device's 23% retained.

The quality of the ITO/ETL interface can also affect C-PSC device performance. Tian et al. (2021) fabricated C-PSCs with a device structure of ITO/APTES-linked C_{60} ETL/$CsMAPbI_3$/CE, in which a self-assembled monolayer of 3-aminopropyl triethoxysilane (APTES) serves as a "molecular glue" to strengthen the adhesion at the ITO/C_{60} ETL interface through chemical interaction and bonding. The research group utilized a premade carbon paste and blade coating for the CE fabrication process. The APTES-modified ITO preserved the integrity of the C_{60} ETL upon blade coating of perovskite layer, resulting in a self-encapsulation effect and reduced hysteresis as well as improved contact quality at the ETL/perovskite film interface to facilitate the interfacial charge extraction and decrease the charged carrier recombination. The champion device had a PCE of 18.64% and retained almost 100% efficiency after 3,000 h in ambient storage without exhibiting measurable degradation, possibly due to the increased hydrophobicity from the self-encapsulation effect of APTES-linked C_{60} ETL.

Xiao et al. (2023) added a tunnel oxide insulating layer at the interface of a mesoporous TiO_2 ETL and perovskite absorber. The resulting HTL free C-PSC with a FTO/c-TiO_2/meso-TiO_2/TOP/$MAPbI_3$/CE device structure demonstrated a PCE of 14.96% with significantly high stability. This champion device was air processed and fabricated with a ZrO_2 tunnel oxide passivating (TOP) layer and a doctor bladed CE. The insulating TOP layer decreased recombination and improved contact at the interface in addition to creating a passivation effect. This resulted in a device with a stability of 88.9% efficiency retained after 11,520 h of ambient storage. Passivation effects within C-PSC device structures reduce layer defect density and increase charged carrier lifetimes, improving device performance (Sun et al., 2021). Figure 4 shows the impressive stability of device parameters over an extended storage period. Xu et al. (2024) incorporated GUA_2SO_4 as a dual interface passivation material within their printable mesoscopic C-PSCs. This passivator primarily affected the buried interface—the interface between the perovskite film and the TiO_2 ETL—and produced low-dimensional perovskite structures near the film grain boundaries. The inclusion of GUA_2SO_4 resulted in improved energy level alignment, carrier extraction, and a device PCE of 18.70%.

Carbon materials can be integrated into other areas of C-PSC device structure in addition to the CE to improve interfacial contact and device performance (Wang Y. et al., 2019; Hui et al., 2020). Wang Y. D. et al. (2022) incorporated defective multi-walled CNTs (D-MWCNTs) into a spiro-OMeTAD HTL, improving the contact quality between the HTL and the graphene CE for rapid charge

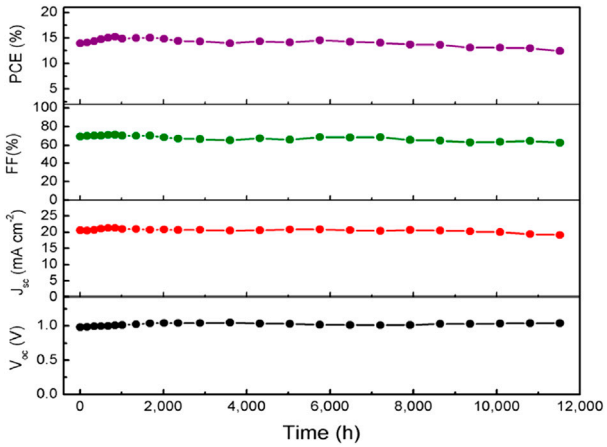

FIGURE 4
Measurement of unencapsulated device photovoltaic parameters over duration of storage in room temperature, dry air at 50% relative humidity (Xiao et al., 2023).

transfer and collection, as seen in Figure 5. This carbon incorporation resulted in a certified PCE of 21.9%, which is the current record efficiency for C-PSCs (Wang Y. D. et al., 2022). The addition of D-MWCNTs allowed improved energy level alignment between the HTL and CE, and the seamless connection between the HTL and carbon electrode increased conductivity at the interface. The device reached a PCE of 22.07% (uncertified) compared to the unaltered spiro-OMeTAD reference device's 17.57% and retained 95% efficiency after 800 h at continuous illumination and MPP tracking.

Carbon quantum dots (CQDs) are nanoscale particles that have high stability and are easily dispersed within solvents (Kim et al., 2020). Tang et al. (2021) used functionalized CQDs to passivate the surface of the $MAPbI_3$ perovskite film surface in their FTO/TiO_2/$MAPbI_3$/CQD/commercial CE structured device. The addition of the CQDs interfacial layer resulted in larger perovskite crystal grains, increased carrier lifetime due to reduced defect density, and favorable energy level alignment. The hydrophobic properties of the device were also improved, which decreased moisture induced degradation. The A-CQD device had a PCE of 13.97% with a stability of 80% efficiency retained after 840 h of storage at 35% relative humidity. Moreover, the incorporation of carbon materials into PSCs shows positive impacts even for devices with metallic electrodes. The same group Xu et al. (2021), incorporated CQDs into the perovskite precursor, the ratio of which was determined through the relative weight of CQD to MAI precursor mass. This modification resulted in the growth of larger $CH_3NH_3PbI_3$ perovskite crystals with less defects for improved charge transport and recombination reduction and a highly hydrophobic surface to improve stability. Liu et al. (2023) embedded CQDs into the SnO_2 ETL of a PSC with a metallic electrode, resulting in improved contact quality and charge transfer at the ETL/perovskite film interface. This method reduced the ETL surface roughness and increased ETL conductivity as well as increasing the grain size of the $FAPbI_3$ based perovskite and creating passivation and energy level alignment effects. The champion device showed a PCE of 24.05% and stability of over 84% efficiency retained after 1,000 h at 1 sun illumination. The device stability was also evaluated in dark storage, in which the device retained 80% efficiency after 500 h at 85°C compared to 65% from the reference device. In addition, the reference device showed significant structural degradation after this test.

4 Manipulation of carbon electrode composition and solvent

4.1 Doping of carbon electrode

Non-carbon materials integrated into the carbon counter electrode layer can serve to improve CE/perovskite contact. CE compositions are often modified to improve the morphology and energy level alignment with the perovskite film (Xiao et al., 2017). Particularly, CE doping is an efficient and scalable way to improve performance of C-PSC devices through the improvement of the CE electrical conductivity and CE/perovskite film interfacial contact, facilitating charge transport and collection. Yu et al. (2024) utilized liquid gallium doping of the commercial paste CE, resulting in a device with a PCE of 13.99% and improved stability compared to the undoped reference device. When doped at a ratio of 1:30 Ga/C and integrated uniformly into the CE, the nontoxic liquid gallium diminished CE surface pores without compromising the CE structural integrity and suppressed nonradiative recombination, improving the contact quality at the CE/perovskite interface. This effect is due to gallium's high conductivity and density; however, at higher ratios overfilling of liquid metal created recombination sites within the CE. The champion liquid gallium doped device had a FTO/$Sn0_2$/$Cs_{0.07}FA_{0.85}MA_{0.14}PbI_{2.57}Br_{0.43}$/CuSCN/CE structure and retained 67% efficiency after 3.5 h at 80°C *versus* the reference device's 58%. In additional tests the unencapsulated champion device retained 65% efficiency after 30 h at 80°C, demonstrating the device's thermal stability. Figure 6 shows the improvement in stability of

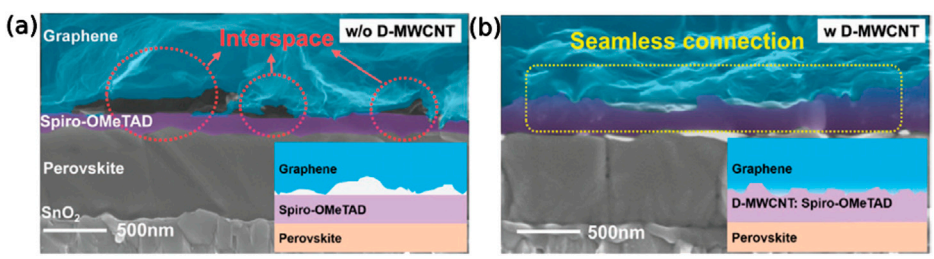

FIGURE 5
Cross-sectional SEM images of devices **(A)** with and **(B)** without D-MWCNT inclusion © 2022 Wiley-VCH GmbH (Wang Y. D. et al., 2022).

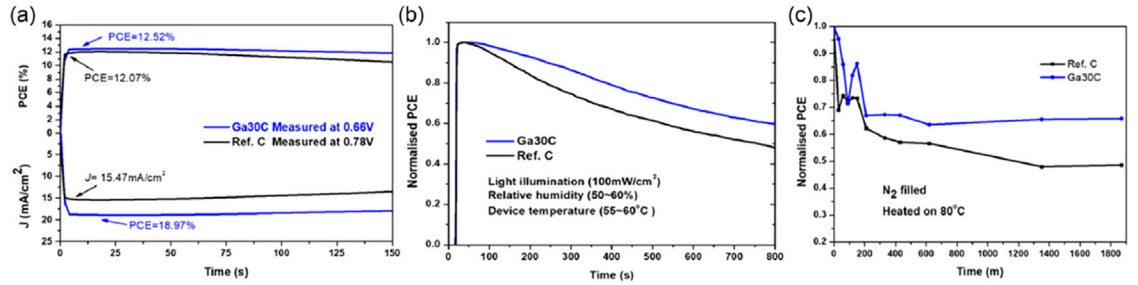

FIGURE 6
(A) Stabilized current density and power outputs under 1 sun illumination. **(B)** Normalized PCE in ambient air conditions at 55°C–60°C with 50%–60% relative humidity under continuous illumination. **(C)** Normalized PCE of thermal stability test in nitrogen at 80°C © 2023 Solar RRL published by Wiley-VCH GmbH (Yu et al., 2024).

the liquid gallium doped PSC compared to the reference device under multiple stability testing conditions, including moisture and temperature stability measurements. Reduction of device stability from ion migration and crystal transformation due to the CuSCN HTL was also reported in the same paper.

Lin et al. (2024) also demonstrated performance improvement from CE doping, utilizing octylammonium iodide (OAI) as dopant in the carbon black and graphite powder CE. The fabricated device had a planar structure of FTO/SnO_2/$FAMAPbI_2$/CE with a PCE value of 19.42%. The OAI doping resulted in a change of the carbon contact angle, increasing the hydrophobicity and creating an internal encapsulating effect. Though the inclusion of OAI dopant did not change the CE conductivity, the doping slightly increased the CE work function—establishing favorable energy level alignment for charge transport and collection. The presence of OAI also affects the perovskite film, creating a layer of 2D perovskite material at the interface and decreasing the perovskite defect density, thereby reducing the recombination at the CE perovskite interface. The unencapsulated champion device retained 80% efficiency after over 450 h in a closed chamber with 85% relative humidity compared to the reference device's 109 h. Figure 7 shows the positive impact of OIA doping on the device performance. At optimal doping level, all photovoltaic parameters related to PCE—including short-circuit current density (Jsc), open-circuit voltage (Voc) and fill factor—were enhanced, demonstrating the benefit of OAI doping on overall C-PSC performance. Gou et al. (2024) doped the CE of their HTL free C-PSC with 30 wt% Mn_3O_4, which allowed the tuning of the CE work function. This improved contact and charge transfer between the perovskite film layer and CE resulted in a PCE of 19.03% compared to the reference device's 10.4%. The CE in the FTO/SnO_2/$MAPbI_3$/PEAI/CE structured device consisted of amorphous carbon black and crystalline graphite and was blade coated. It was also observed to be denser with the addition of Mn_3O_4, improving the connections within the CE. The champion device was fabricated with a PEAI passivation layer and retained 90% of its initial PCE after 2000 h of storage in environmental conditions.

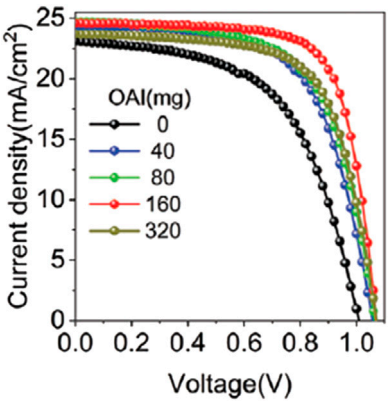

FIGURE 7
Planar C-PSC current density vs. voltage curves with varying levels of OAI dopant © 2022 Wiley-VCH GmbH (Lin et al., 2024).

4.2 Carbon solvent selection to prevent perovskite film degradation

An aspect of C-PSC production that affects each of the aforementioned interface modification methods is the interaction between the perovskite film and carbon solvents used during device fabrication. CEs are composed of carbon, binders, and solvents—the properties of each having a significant impact on the behavior of the resulting carbon contact material (Tsuji et al., 2023). The choice of carbon solvent influences perovskite film morphology and crystallization quality at the perovskite film/CE interface (Chen et al., 2016). Poor perovskite film/solvent compatibility can significantly degrade or even damage the perovskite lattice, lowering contact quality between layers as well as overall PSC performance. Though this can occur from interaction with any solvent or binder used during device fabrication, the solvents and binders utilized in the CE paste formulation are especially impactful (Xie et al., 2020). Polar solvents in particular can lead to harmful degradation of the underlying perovskite film (Hwang et al., 2015). As such, the components of each C-PSC layer and their respective elements must be carefully evaluated to avoid degradation within the device.

Kartikay et al. (2020) studied HTL free C-PSCs with different carbon solvents and binders to evaluate the compatibility between the resulting CE and perovskite film layer. The binders chosen were ethyl cellulose (EC), PMMA, and PVP and the solvents utilized included chlorobenzene, toluene, and terpineol. The CEs in the ITO/c-TiO_2/m-TiO_2/$FA_{1-x}MA_xPbI_{3-y}Br_y$/CE structured devices were

composed of carbon black and graphite and were ~5 μm thick. The group reported that the CEs based on the PMMA binder had a better distribution of carbon particles and higher conductivities than the PVP-based CEs, which also showed higher rates of perovskite film degradation. Xie et al. (2020) obtained positive results in CE/perovskite film compatibility by using low polar alkane solvents, avoiding polar CE components. Jiang et al. (2018) fabricated highly compatible CEs by adding TTIP and acetic acid in the CE paste, resulting in CEs with improved conductivity and electrical interconnection as well as a homogeneous perovskite film surface. Further investigations on the compatibility between the perovskite film and CE solvents/binders are necessary to avoid degradation, improve contact quality, and reduce losses at the CE/perovskite interface.

5 Control of perovskite crystallization

The contact quality and electrical characteristics of the CE/perovskite film interface can also be improved through crystallization control of the perovskite material. Increases in the grain size of perovskite crystals generally improve perovskite film quality and overall device performance (Chen et al., 2022). Grain boundary reduction has been shown to increase charged carrier lifetime, decreasing charge carrier losses from nonradiative recombination (Wu et al., 2021). Li L. C. et al. (2023) fabricated ambient air processed, HTL free C-PSCs with a PCE of 17.69% including spin coated $FA_{0.6}Cs_{0.4}PbI_3$ perovskite film in a FTO/TiO_2/perovskite/commercial CE structure. This group added FAAc to the perovskite precursor, which reduced the formation of intermediate (1D) perovskite crystals and facilitated creation of high-quality, pinhole defect free film. The incorporation of FAAc resulted in the formation of large perovskite grains (2-3 μm), thereby reducing the device defect density and nonradiative recombination. The FAAc molecules decomposed during the annealing process and do not affect the perovskite lattice structure. The champion FAAc treated device achieved a stability of 92% efficiency retained after 1,000 h as an unencapsulated device in an ambient environment with 20%–25% relative humidity. In addition, this crystallization control method positively impacted the ambient air processing of the formamidine based perovskite, which was noted to be a difficult task without the FAAc treatment. This study demonstrates the benefit of perovskite crystallization control on the CE/perovskite interface characteristics, device performance, and fabrication scalability.

Wang W. R. et al. (2024) manipulated the perovskite crystallization with dimethylamine oxalate, resulting in improved film morphology and a PCE of 18.84%. Dimethylamine oxalate was added into the $CsPbI_3$ perovskite precursor of the FTO/TiO_2/perovskite/CE structured devices. The champion device demonstrated increased perovskite grain size, reduced defect density, and decreased hysteresis. Xiang et al. (2024) added a multifunctional fluorinated molecule, 6FDA, to the perovskite precursor of a printable mesoscopic C-PSC to improve the perovskite crystallization. The addition of 6FDA enhanced the hydrophobicity of the perovskite film and created a passivation effect, resulting in a PCE of 20.15%. Due to the inclusion of 6FDA, the interfacial charged carrier recombination was reduced in the FTO/c-TiO_2/m-TiO_2/CsFAMA perovskite/m-ZrO_2/commercial CE structured device, specifically improving charge extraction between the perovskite absorber and ETL. Under ambient air, MPP tracking stability testing conditions of approximately 55°C at 50% relative humidity the encapsulated 6FDA device retained 90% of its PCE after 640 h, demonstrating reduced perovskite degradation over time compared to the reference device.

Du et al. (2024) manipulated the crystallization of $CsFAPbI_3$ by reformulating the perovskite precursor, using pre-synthesized single crystals rather than powders. In creating perovskite precursor with increased ink volatility, this group also increased the size of the perovskite grains and reduced the presence of defect clusters. The process of gas quenching treatment of the perovskite film is cited to be one of the most significant factors on the quality of the film's morphology. The champion ITO/SnO_2/$CsFAPbI_3$/TaTm/PEDOT/commercial CE structured device demonstrated a PCE of 19.3% and retained 80% of its initial PCE after 1,000 h at MMP tracking in 85°C and under 1 sun illumination. The performance of the crystallization-controlled PSCs was drastically improved from that of the reference device, which reached 80% of its initial PCE after 200 h under the same conditions. The switch to pre-synthesized single crystals reduced the presence of insoluble impurities within the perovskite precursor and reduced the perovskite precursor material costs by as much as 80%.

Yang et al. (2021) utilized a PDCBT/Ta-WO_x HTL in their ITO/SnO_2/$MAGAPbI_3$/PDCBT/Ta-WO_x/CE structured device. The fully printed, solution processed device was fabricated in ambient conditions and resulted in a PCE of 18.1%. GACl was added to the perovskite precursor, which increased the perovskite grain size and consequently improved the layer's diffusion length, reduced carrier recombination, and increased hydrophobicity. Under stability testing in ambient atmosphere and 30% relative humidity, the unencapsulated device retained 100% of its initial PCE after 5,000 h, whereas the metallic electrode device retained less than 40% of its PCE after 300 h. This significant stability improvement approved the effectiveness of the proposed device engineering strategies.

In addition to the incorporation of additives into perovskite precursors to improve the crystallization of perovskite thin films, other strategies were also developed. Li et al. (2024) utilized the presence of moisture to trigger secondary perovskite crystal growth through the formation of intermediates. The moisture-induced secondary crystal growth improved the crystalline quality and optimized the energy level of perovskite film for favorable alignment with CE contact, resulting in a HTL free C-PSC device with a 19.52% PCE. Formation of metastable intermediates is typically regarded harmful for perovskite crystallization. For instance, the suppression of intermediate formation during perovskite crystallization is a means for improving the performance of all-inorganic PSCs, with Liu et al. (2020) reporting increased grain size of $CsPbI_2Br$ perovskite film after treatment with a lead reactant. Here the intermediates were demonstrated to trigger secondary crystal growth, which improved crystallinity, enlarged grain sizes, and created better quality morphology in the perovskite films, thereby reducing the defect density and nonradiative recombination. The secondary growth also modulated the surface composition to attain favorable energy level alignment for charge transport and collection. Control of the 2D and 3D crystallization proportion of the perovskite composition has also been applied in other studies to affect energy level alignment at the CE/perovskite film interface as well as C-PSC device

TABLE 1 Summary of devices referenced.

Interface modification category	Device structure/Information	PCE	Stability test duration	Stability test conditions	Stability test PCE retention (%)	Ref
CE Doping	FTO/$Sn0_2$/$Cs_{0.07}FA_{0.85}MA_{0.14}PbI_{2.57}Br_{0.43}$/CuSCN/CE	13.99%	30 h	Unencapsulated device at 80°C	65	Yu et al. (2024)
CE Doping	FTO/SnO_2/$MAPbI_3$/PEAI/CE	19.03%	2000 h	Storage in environmental conditions	90	Gou et al. (2024)
CE Doping	FTO/SnO_2/$FAMAPbI_2$/CE	19.42%	450 h	Unencapsulated device at 85% RH	80	Lin et al. (2024)
Crystallization Control	FTO/TiO_2/$FA_{0.6}Cs_{0.4}PbI_3$/CE	17.69%	1,000 h	Unencapsulated device at 20%–25% RH	92	Li Y. Q et al. (2023)
Crystallization Control	ITO/SnO_2/$MAGAPbI_3$/PDCBT/Ta-WO_x/CE	18.1%	5,000 h	Ambient atmosphere at 30% RH	100	Yang et al. (2021)
Crystallization Control	FTO/TiO2/$CsPbI_3$/CE	18.84%				Wang W. R et al. (2024)
Crystallization Control	ITO/SnO_2/$CsFAPbI_3$/TaTm/PEDOT/CE	19.3%	1,000 h	MPP tracking at 85°C	80	Du et al. (2024)
Crystallization Control	FTO/TiO2/ZrO2/CE scaffold filled with $MAPbI_3$ perovskite via drop coating	19.35%				Cheng et al. (2023)
Crystallization Control	FTO/c-TiO_2/m-TiO_2/$CsPbI_2Br$/CE	19.52%				Li et al. (2024)
Crystallization Control	FTO/c-TiO_2/m-TiO_2/CsFAMA perovskite/m-ZrO_2/CE	20.15%	640 h	MPP tracking at 55°C and 50% RH	90	Xiang et al. (2024)
Interface Layer/Treatment	D-MWCNTs incorporated into spiro-OMeTAD HTL	22.07% (21.9% cert.)	800 h	MPP tracking	95	Wang Y. D et al. (2022)
Interface Layer/Treatment	perovskite/ZnPc and $CsPbBr_3$ perovskite quantum dots/CE	10.20%	4,380 h	Unencapsulated device at ~30% RH	99.50	Zou et al. (2023)
Interface Layer/Treatment	A-CQD, FTO/TiO_2/$MAPbI_3$/IPA/CE	13.97%	840 h	Storage at 35% RH	80	Tang et al. (2021)
Interface Layer/Treatment	FTO/c-TiO_2/meso-TiO_2/TOP/$MAPbI_3$/CE	14.96%	11,520 h	Ambient storage	88.90	Xiao et al. (2023)
Interface Layer/Treatment	ITO/SnO_2/$FAMAPbI_3$/KLA/CE	16.10%	1,440 h	Ambient storage at 20°C–25°C and 50%–60% RH	85	Zhang et al. (2024b)
Interface Layer/Treatment	ITO/SnO_2/$FAMAPbI_3$/CE	16.56%	700 h	Ambient storage at ~20°C and 20%–60% RH	~80	Tang et al. (2024)
Interface Layer/Treatment	ITO/SnO_2/FABr/$MAPbI_3$/CE/FAI	17.49%	1,440 h	Ambient storage	96	Li S. Q et al. (2023)
Interface Layer/Treatment	Carbon ET, ITO/APTES-linked C_{60}/$CsMAPbI_3$/CE	18.64%	3,000 h	Ambient storage	~100	Tian et al. (2021)
Interface Layer/Treatment	GUA_2SO_4 at ETL/perovskite interface	18.70%				Xu et al. (2024)
Interface Layer/Treatment	$FA_{0.4}MA_{0.6}PbI_3$/CATNI/CE	18.90%	1,000 h	Dark conditions at 30°C and 30% RH	95.50	Wang W. R et al. (2024)

(Continued on following page)

TABLE 1 (*Continued*) Summary of devices referenced.

Interface modification category	Device structure/Information	PCE	Stability test duration	Stability test conditions	Stability test PCE retention (%)	Ref
Interface Layer/Treatment	$FA_{0.6}MA_{0.4}PbI_3$, CTAB doped NiOx	20.14%	275 h	At maximum power point	95	Li Y. Q et al. (2023)
Interface Layer/Treatment	ITO/SnO_2/$MAPBI_3$/P3HT/NiOx/CE	20.80%	300 h	Ambient air with 40%–50% RH	80	Lu et al. (2023)
Interface Layer/Treatment - Metallic PSCs	$CH_3NH_3PbI_3$ perovskite, A-CQD	13.28%	200 h		90	Xu et al. (2021)
Interface Layer/Treatment - Metallic PSCs	FTO/SnO2 with CQDs/$FAPbI_3$/spiro-OMeTAD/Au	24.05%	1,000 h	1 sun illumination	84	Liu et al. (2023)
PSM	$FA_{0.4}MA_{0.6}PbI_3$/CATNI/CE, 25 cm^2 area	14.60%				Wang H. L et al. (2024)
PSM	ITO/SnO_2/$MAGAPbI_3$/P3HT/CE PSM, 25 cm^2 area	15.3%				Yang et al. (2021)
PSM	6FDA treated, 56.4 cm^2 area	15.41%				Xiang et al. (2024)
PSM	ITO/SnO_2/$CsFAPbI_3$/TaTm/PEDOT/CE, 25 cm^2 area	16.2%				Du et al. (2024)
PSM	FTO/TiO2/ZrO2/CE scaffold filled with $MAPbI_3$ perovskite via drop coating, 52.3 cm^2 area	16.53%	600 h	Continuous work at ~55°C	93	Cheng et al. (2023)

performance and stability (Schmitz et al., 2024; Almalki et al., 2024; Wang H. L. et al., 2022). Another group, Cheng et al. (2023) utilized perovskite crystallization control to improve film homogeneity in printed mesoscopic C-PSCs without HTLs. In this process a chamber was built on the wet $MAPbI_3$ perovskite precursor to control the solvent vapor removal process. The crystal orientation was directed and the film homogeneity increased through the method's pore filling effect. The champion PSC had a commercial carbon paste CE and a recorded PCE of 19.35% for a 1 cm^2 area. This scalable perovskite crystallization control method exhibited improvement of device performance, stability, and production scalability.

6 Production and commercialization of carbon-based perovskite solar modules (PSMs)

Continued advances in PSCs with carbon electrodes create a positive outlook for improving the producibility and quality of PSMs. Various previously discussed interfacial engineering methods applied to C-PSCs were also utilized in PSM fabrication. The interface modification demonstrated by Wang H. L. et al. (2024) utilizing CATNI was also applied to production of a four-unit module PSM, which had an area of 25 cm^2 and an efficiency of 14.6%. Crystallization control was applied to PSM fabrication by Cheng et al. (2023) which resulted in a PCE of 16.53% for a 52.3 cm^2 area module and a stability of 93% efficiency retained after 600 h of continuous work at approx. 55°C. Xiang et al. (2024) applied the crystallization control and passivation effect created by 6FDA incorporation to a 56.4 cm^2 area PSM, which resulted in a PCE of 15.41%. Du et al. (2024) fabricated a PSM with their pre-synthesized single crystal perovskite precursor. The PSMs demonstrated an active-area PCE of 16.2% over 25 cm^2. Yang et al. (2021) also used the GACl perovskite precursor addition to fabricate a 25 cm^2, ITO/SnO_2/$MAGAPbI_3$/P3HT/CE structured PSM. This resulted in a four-cell PSM with a PCE of 15.3% and high potential for large scale, roll-to-roll production.

There are a great many challenges currently hindering the widespread commercialization of C-PSMs. Fabrication methods for PSCs must be adapted to large device areas while retaining sustainable costs and scalable production (Weerasinghe et al., 2024). Some of the primary limitations for PSM production include the homogeneity and quality of large area thin films and the degradation of perovskite material at cell interconnection areas. These drawbacks necessitate progress in the quality, consistency, and scalability of perovskite device production in order to improve PSM efficiency and cost. The use of CEs greatly decreases the cost of materials and production compared to that of metallic electrodes and increases production scalability through the feasibility of low-temperature device fabrication with simplified solution processes. C-PSCs also have the prospect of high stability because of increased hydrophobicity, restricted carbon diffusion into perovskite, or even encapsulation effects due to the inclusion of the carbon contact in the device structure. Herein, C-PSC interface modification methods show significant promise in the improvement of device efficiency and stability, of which the increased performance consistency of both has substantial potential for the further development of PSMs. Table 1 summarizes the performance of all C-PSCs referenced.

7 Conclusions and outlook

The use of CEs in PSC production has marked advantages over that of metallic electrodes, and the main disadvantage—poor contact quality at the CE/perovskite film interface—could be minimized with further advances in interface modification. The application of interface modification methods such as interface layer additions and treatments, CE doping and solvent choice, and crystallization control of perovskite films in C-PSC fabrication has resulted in the improvement of device efficiency and long-term stability. Favorable results from interfacial engineering in C-PSCs include the increase of contact quality between layers, CE conductivity, energy level alignment, and defect passivation effects. The improvements resulting from interface modifications show great promise in the future development of C-PSC technology as well as in the large-scale production of PSMs.

The specific topic of interface modifications in C-PSCs, as well as the research development areas of C-PSC technology in general, holds significant potential for advances and commercialization in perovskite-based photovoltaics. Based on the information assessed in this review, there are multiple areas of inquiry that are recommended for future research directions. The use of low-temperature C-PSC structures—including those with planar architectures, no HTL, or otherwise simplified structures—allow for cost-effective mass production of PSC and PSM devices. Fabrication techniques with the means for large-scale production such as layer-by-layer deposition, solution processibility, and fully printable devices are essential for the continued expansion of C-PSC technology's feasibility.

Explicit consideration of the material properties of device components during development, especially with focus on material compatibility, encourages high-quality, high consistency production. This can be applied to the properties of any device layer, such as the CE morphology related to compositional factors and the interaction between the perovskite material and carbon solvents and binders utilized during fabrication. For interface modification in particular, high promise directions include the methods of CE doping, the addition and treatments of the interface buffer layer, favorable energy level alignment, crystallization control, and carbon integration. Simultaneous modification of multiple layer interfaces also shows noteworthy results for enhancing CE/perovskite film interface quality, passivating defects to reduce nonradiative recombination, and establishing favorable energy level alignment for charge transport and collection. Utilization of one or more of these methods with resulting improvements in layer contact quality, passivation effects, and increases in hydrophobicity especially shows substantial promise for advances in C-PSC stability, which is currently a major barrier to the commercial viability of perovskite-based solar technology. Each of these suggestions for the outlook of C-PSC research advancements can be applied further to the design, production, and progress of PSM technologies.

Author contributions

MB: Formal Analysis, Investigation, Methodology, Writing–original draft. DL: Conceptualization, Formal Analysis, Methodology, Supervision, Writing–review and editing.

Funding

The author(s) declare that financial support was received for the research, authorship, and/or publication of this article. This work was supported by the U.S. Department of Energy's Office of Energy Efficiency and Renewable Energy (EERE) under the Solar Energy Technologies Office Award Number DE-EE0010242. This study was also partially supported by the National Aeronautics and Space Administration, Alabama EPSCoR International Space Station Flight Opportunity program (contract# 80NSSC20M0141).

Conflict of interest

The authors declare that the research was conducted in the absence of any commercial or financial relationships that could be construed as a potential conflict of interest.

Publisher's note

References

Aji, D., Darsono, N., Roza, L., Khaerudini, D. S., and Timuda, G. E. (2024). Bibliometric analysis of carbon-based electrode perovskite solar cells progress. *Sol. Energy* 274, 112587. doi:10.1016/j.solener.2024.112587

Almalki, M., Alotaibi, M. H., Alanazi, A. Q., Eickemeyer, F. T., Alenzi, S. M., Alzahrani, Y. A., et al. (2024). Interfacial modulation through mixed-dimensional heterostructures for efficient and hole conductor-free perovskite solar cells. *Adv. Funct. Mater.* 34 (6). doi:10.1002/adfm.202309789

Aung, S. K. K., Vijayan, A., Seetawan, T., and Boschloo, G. (2022). Improved efficiency of perovskite solar cells with low-temperature-processed carbon by introduction of a doping-free polymeric hole conductor. *Sol. Rrl* 6 (8). 2100773. doi:10.1002/solr.202100773

Baranwal, A. K., Kanaya, S., Peiris, T. A. N., Mizuta, G., Nishina, T., Kanda, H., et al. (2016). 100°C thermal stability of printable perovskite solar cells using porous carbon counter electrodes. *Chemsuschem* 9 (18), 2604–2608. doi:10.1002/cssc.201600933

Beynon, D., Parvazian, E., Hooper, K., McGettrick, J., Patidar, R., Dunlop, T., et al. (2023). All-printed roll-to-roll perovskite photovoltaics enabled by solution-processed carbon electrode. *Adv. Mater.* 35 (16). doi:10.1002/adma.202208561

Bidikoudi, M., and Stathatos, E. (2023). Carbon electrodes: the rising star for PSC commercialization. *Electronics* 12 (4), 992. doi:10.3390/electronics12040992

Bogachuk, D., Zouhair, S., Wojciechowski, K., Yang, B., Babu, V., Wagner, L., et al. (2020). Low-temperature carbon-based electrodes in perovskite solar cells. *Energy and Environ. Sci.* 13 (11), 3880–3916. doi:10.1039/d0ee02175j

Boyd, C. C., Cheacharoen, R., Leijtens, T., and McGehee, M. D. (2019). Understanding degradation mechanisms and improving stability of perovskite photovoltaics. *Chem. Rev.* 119 (5), 3418–3451. doi:10.1021/acs.chemrev.8b00336

Calabrò, E., Matteocci, F., Paci, B., Cinà, L., Vesce, L., Barichello, J., et al. (2020). Easy strategy to enhance thermal stability of planar PSCs by perovskite defect passivation and

low-temperature carbon-based electrode. *Acs Appl. Mater. and Interfaces* 12 (29), 32536–32547. doi:10.1021/acsami.0c05878

Chen, C., Bala, H., Yao, S., Zhang, B., Sha, N., An, X., et al. (2022). Enhanced efficiency and stability of perovskite solar cells based on carbon-counter-electrode via anti-solvent treatment. *J. Alloys Compd.* 920, 165874. doi:10.1016/j.jallcom.2022.165874

Chen, H. N., and Yang, S. H. (2019). Methods and strategies for achieving high-performance carbon-based perovskite solar cells without hole transport materials. *J. Mater. Chem. A* 7 (26), 15476–15490. doi:10.1039/c9ta04707g

Chen, H. N., and Yang, S. H. (2017). Carbon-based perovskite solar cells without hole transport materials: the front runner to the market? *Adv. Mater.* 29 (24), 1603994. doi:10.1002/adma.201603994

Chen, J. Z., Xiong, Y., Rong, Y., Mei, A., Sheng, Y., Jiang, P., et al. (2016). Solvent effect on the hole-conductor-free fully printable perovskite solar cells. *Nano Energy* 27, 130–137. doi:10.1016/j.nanoen.2016.06.047

Chen, W., Yin, X., Que, M., Xie, H., Liu, J., Yang, C., et al. (2019). A comparative study of planar and mesoporous perovskite solar cells with printable carbon electrodes. *J. Power Sources* 412, 118–124. doi:10.1016/j.jpowsour.2018.11.031

Cheng, Y., and Lin, F. (2022). "Semitransparent perovskites for solar cells and smart windows," in *Perovskite materials and devices*, 349–377.

Cheng, Y. J., Zheng, Z., Liu, S., Xiang, J., Han, C., Xia, M., et al. (2023). Scalable in-plane directional crystallization for the printable hole-conductor-free perovskite solar cell based on the carbon electrode. *Adv. Energy Mater.* 14. doi:10.1002/aenm.202303988

Chu, Q. Q., Sun, Z. J., Ding, B., Moon, K. S., Yang, G. J., and Wong, C. P. (2020). Greatly enhanced power conversion efficiency of hole-transport-layer-free perovskite solar cell via coherent interfaces of perovskite and carbon layers. *Nano Energy* 77, 105110. doi:10.1016/j.nanoen.2020.105110

Dong, Q. S., Zhu, C., Chen, M., Jiang, C., Guo, J., Feng, Y., et al. (2021). Interpenetrating interfaces for efficient perovskite solar cells with high operational stability and mechanical robustness. *Nat. Commun.* 12 (1), 973. doi:10.1038/s41467-021-21292-3

Du, T., Rehm, V., Qiu, S., Pal, S., Jang, D., Peng, Z., et al. (2024). Precursor-engineered volatile inks enable reliable blade-coating of cesium-formamidinium perovskites toward fully printed solar modules. *Adv. Sci.* 11, e2401783. doi:10.1002/advs.202401783

Fagiolari, L., and Bella, F. (2019). Carbon-based materials for stable, cheaper and large-scale processable perovskite solar cells. *Energy and Environ. Sci.* 12 (12), 3437–3472. doi:10.1039/c9ee02115a

Gan, Y. Q., Sun, J., Guo, P., Jiang, H., Li, J., Zhu, H., et al. (2023). Advances in the research of carbon electrodes for perovskite solar cells. *Dalton Trans.* 52 (45), 16558–16577. doi:10.1039/d3dt03136e

González, L. M., Ramirez, D., and Jaramillo, F. (2022). Current status and trends of carbon-based electrodes for fully solution-processed perovskite solar cells. *J. Energy Chem.* 68, 222–246. doi:10.1016/j.jechem.2021.11.020

Gou, Y. Z., Zhang, J., Jin, B., Dai, W., Zhang, W., Chen, C., et al. (2024). Work function tuning of carbon electrode to boost the charge extraction in hole transport layer-free perovskite solar cells. *Small* 20, e2403342. doi:10.1002/smll.202403342

Grancini, G., Roldán-Carmona, C., Zimmermann, I., Mosconi, E., Lee, X., Martineau, D., et al. (2017). One-Year stable perovskite solar cells by 2D/3D interface engineering. *Nat. Commun.* 8, 15684. doi:10.1038/ncomms15684

He, R., Huang, X. Z., Chee, M., Hao, F., and Dong, P. (2019). Carbon-based perovskite solar cells: from single-junction to modules. *Carbon Energy* 1 (1), 109–123. doi:10.1002/cey2.11

Hui, W., Yang, Y., Xu, Q., Gu, H., Feng, S., Su, Z., et al. (2020). Red-carbon-quantum-Dot-doped SnO_2 composite with enhanced electron mobility for efficient and stable perovskite solar cells. *Adv. Mater.* 32 (4), 1906374. doi:10.1002/adma.201906374

Hwang, I., Jeong, I., Lee, J., Ko, M. J., and Yong, K. (2015). Enhancing stability of perovskite solar cells to moisture by the facile hydrophobic passivation. *Acs Appl. Mater. and Interfaces* 7 (31), 17330–17336. doi:10.1021/acsami.5b04490

Jiang, P., Jones, T. W., Duffy, N. W., Anderson, K. F., Bennett, R., Grigore, M., et al. (2018). Fully printable perovskite solar cells with highly-conductive, low-temperature, perovskite-compatible carbon electrode. *Carbon* 129, 830–836. doi:10.1016/j.carbon.2017.09.008

Kartikay, P., Yella, A., and Mallick, S. (2020). Binder-solvent effects on low temperature-processed carbon-based, hole-transport layer free perovskite solar cells. *Mater. Chem. Phys.* 256, 123594. doi:10.1016/j.matchemphys.2020.123594

Kim, J. K., Nguyen, D. N., Lee, J. H., Kang, S., Kim, Y., Kim, S. S., et al. (2020). Carbon quantum dot-incorporated nickel oxide for planar p-i-n type perovskite solar cells with enhanced efficiency and stability. *J. Alloys Compd.* 818, 152887. doi:10.1016/j.jallcom.2019.152887

Li, L. C., Rao, H., Wu, Z., Hong, J., Zhang, J., Pan, Z., et al. (2024). Moisture induced secondary crystal growth boosting the efficiency of hole transport layer-free carbon-based perovskite solar cells beyond 19.5%. *Adv. Funct. Mater.* 34 (1). doi:10.1002/adfm.202308428

Li, L. C., Zhang, R., Wu, Z., Wang, Y., Hong, J., Rao, H., et al. (2023). Crystallization control of air-processed wide-bandgap perovskite for carbon-based perovskite solar cells with 17.69% efficiency. *Chem. Eng. J.* 455, 140566. doi:10.1016/j.cej.2022.140566

Li, S. Q., Li, Y., Sun, X. N., Li, Y., Deng, F., and Tao, X. (2023). Hole transport layer-free carbon-based perovskite solar cells with high-efficiency up to 17.49% in air: from-bottom-to-top perovskite interface modification. *Chem. Eng. J.* 455, 140727. doi:10.1016/j.cej.2022.140727

Li, Y. H., Xie, H. B., Lim, E. L., Hagfeldt, A., and Bi, D. Q. (2022). Recent progress of critical interface engineering for highly efficient and stable perovskite solar cells. *Adv. Energy Mater.* 12 (5). 2102730. doi:10.1002/aenm.202102730

Li, Y. Q., Lu, X., Mei, Y., Dong, C., Gangadharan, D. T., Liu, K., et al. (2023). Blade-coated carbon electrode perovskite solar cells to exceed 20% efficiency through protective buffer layers. *Adv. Funct. Mater.* 33 (34). doi:10.1002/adfm.202301920

Lin, H. S., Okawa, S., Ma, Y., Yotsumoto, S., Lee, C., Tan, S., et al. (2020). Polyaromatic nanotweezers on semiconducting carbon nanotubes for the growth and interfacing of lead halide perovskite crystal grains in solar cells. *Chem. Mater.* 32 (12), 5125–5133. doi:10.1021/acs.chemmater.0c01011

Lin, S. Y., Fang, Z., Ma, J., Guo, D., Yu, X., Xie, H., et al. (2024). Octylammonium iodide induced in-situ healing at "perovskite/carbon" interface to achieve 85% RH-moisture stable, hole-conductor-free perovskite solar cells with power conversion efficiency >19%. *Small Methods* 8 (1), 2300716. doi:10.1002/smtd.202300716

Ling, X. F., Zhou, S., Yuan, J., Shi, J., Qian, Y., Larson, B. W., et al. (2019). 14.1% $CsPbI_3$ perovskite quantum dot solar cells via cesium cation passivation. *Adv. Energy Mater.* 9 (28). 1900721. doi:10.1002/aenm.201900721

Liu, C., Wu, M., Wu, Y. C., Wang, D. F., and Zhang, T. J. (2020). Efficient all-inorganic $CsPbI_2Br$ perovskite solar cell with carbon electrode by revealing crystallization kinetics and improving crystal quality. *J. Power Sources* 447, 227389. doi:10.1016/j.jpowsour.2019.227389

Liu, J., Yin, Y., He, B., Wang, P., Wang, M., Cai, W., et al. (2023). Focusing on the bottom contact: carbon quantum dots embedded SnO2 electron transport layer for high-performance and stable perovskite solar cells. *Mater. Today Phys.* 33, 101041. doi:10.1016/j.mtphys.2023.101041

Lu, X. Y., Li, Y., Dong, C., Gao, Y., Yue, G., Liu, K., et al. (2023). Efficient carbon electrode perovskite solar cells with robust buffer interfaces. *J. Mater. Res. Technology-Jmr&T* 24, 8162–8170. doi:10.1016/j.jmrt.2023.05.038

Maniarasu, S., Korukonda, T. B., Manjunath, V., Ramasamy, E., Ramesh, M., and Veerappan, G. (2018). Recent advancement in metal cathode and hole-conductor-free perovskite solar cells for low-cost and high stability: a route towards commercialization. *Renew. and Sustain. Energy Rev.* 82, 845–857. doi:10.1016/j.rser.2017.09.095

McMeekin, D. P., Mahesh, S., Noel, N. K., Klug, M. T., Lim, J., Warby, J. H., et al. (2019). Solution-processed all-perovskite multi-junction solar cells. *Joule* 3 (2), 387–401. doi:10.1016/j.joule.2019.01.007

Meng, F. N., Liu, A., Gao, L., Cao, J., Yan, Y., Wang, N., et al. (2019). Current progress in interfacial engineering of carbon-based perovskite solar cells. *J. Mater. Chem. A* 7 (15), 8690–8699. doi:10.1039/c9ta01364d

Meng, F. N., Wang, D. S., Chang, J. R., Li, J. H., and Wang, G. Q. (2024). Application of carbon materials in conductive electrodes for perovskite solar cells. *Sol. Rrl* 8 (6). doi:10.1002/solr.202301030

Nazir, G., Lee, S., Lee, J., Rehman, A., Lee, J., Seok, S. I., et al. (2022). Stabilization of perovskite solar cells: recent developments and future perspectives. *Adv. Mater.* 34 (50). doi:10.1002/adma.202204380

Niu, G. D., Li, W. Z., Li, J. W., and Wang, L. D. (2016). Progress of interface engineering in perovskite solar cells. *Sci. China-Materials* 59 (9), 728–742. doi:10.1007/s40843-016-5094-6

NREL. *Best research-cell efficiency chart*. Golden, CO: NREL. Available at: https://www.nrel.gov/pv/cell-efficiency.html (Accessed June 17, 2024).

Pandey, S., Karakoti, M., Bhardwaj, D., Tatrari, G., Sharma, R., Pandey, L., et al. (2023). Recent advances in carbon-based materials for high-performance perovskite solar cells: gaps, challenges and fulfillment. *Nanoscale Adv.* 5 (6), 1492–1526. doi:10.1039/d3na00005b

Peng, C., Su, H., Li, J., Duan, Q., Li, Q., Xiao, J., et al. (2021). Scalable, efficient and flexible perovskite solar cells with carbon film based electrode. *Sol. Energy Mater. Sol. Cells* 230, 111226. doi:10.1016/j.solmat.2021.111226

Qiu, J. H., and Yang, S. H. (2020). Material and interface engineering for high-performance perovskite solar cells: a personal journey and perspective. *Chem. Rec.* 20 (3), 209–229. doi:10.1002/tcr.201900028

Qiu, L. B., He, S. S., Ono, L. K., Liu, S. Z., and Qi, Y. B. (2019). Scalable fabrication of metal halide perovskite solar cells and modules. *Acs Energy Lett.* 4 (9), 2147–2167. doi:10.1021/acsenergylett.9b01396

Schmitz, F., Bhatia, R., Burkhart, J., Schweitzer, P., Allione, M., Gallego, J., et al. (2024). Improved hole extraction and band alignment via interface modification in hole transport material-free Ag/Bi double perovskite solar cells. *Sol. Rrl* 8 (6). doi:10.1002/solr.202300965

Sulistianto, J., Konno, A., Abuzairi, T., and Poespawati, N. R. (2024). Perovskite solar cells with modified carbon electrode and CuSCN interlayer processed under ambient conditions. *Int. J. Photoenergy* 2024 (1), 5355903. doi:10.1155/2024/5355903

Sun, M. R., Zhu, J., He, B., Bu, F., Ti, J., Yao, X., et al. (2021). Efficient defect passivation and charge extraction with hexamethylenetetramine interface modification

for hole-transporting layers-free $CsPbBr_3$ perovskite solar cells. *Sol. Rrl* 5 (8), 2100344. doi:10.1002/solr.202100344

Tang, H. B., Xu, T., Qin, X., Zou, K., Lv, S., Fan, J., et al. (2021). Carbon quantum dot-passivated perovskite/carbon electrodes for stable solar cells. *Acs Appl. Nano Mater.* 4 (12), 13339–13351. doi:10.1021/acsanm.1c02850

Tang, S. W., Zong, P., Zhong, J., He, F., Cheng, N., Hang, F., et al. (2024). Efficient carbon-based perovskite solar cells passivated by alkylammonium chloride. *Sol. Rrl* 8 (3). doi:10.1002/solr.202300854

Tian, T., Zhong, J., Yang, M., Feng, W., Zhang, C., Zhang, W., et al. (2021). Interfacial linkage and carbon encapsulation enable full solution-printed perovskite photovoltaics with prolonged lifespan. *Angew. Chemie-International Ed.* 60 (44), 23735–23742. doi:10.1002/anie.202108495

Tountas, M., Polyzoidis, C., Loizos, M., Rogdakis, K., and Kymakis, E. (2023). Improved performance of hole-transporting material-free perovskite solar cells using a low-temperature printed carbon paste. *Acs Appl. Electron. Mater.* 5 (11), 6228–6235. doi:10.1021/acsaelm.3c01132

Tsuji, R., Tanaka, K., Oishi, K., Shioki, T., Satone, H., and Ito, S. (2023). Role and function of polymer binder thickeners in carbon pastes for multiporous-layered-electrode perovskite solar cells. *Chem. Mater.* 35 (20), 8574–8589. doi:10.1021/acs.chemmater.3c01483

Wang, H. L., Liu, H., Dong, Z., Wei, X., Song, Y., Li, W., et al. (2022). Extracting ammonium halides by solvent from the hybrid perovskites with various dimensions to promote the crystallization of $CsPbI_3$ perovskite. *Nano Energy* 94, 106925. doi:10.1016/j.nanoen.2022.106925

Wang, H. L., Liu, H. C., Li, W. P., Zhu, L. Q., and Chen, H. N. (2020). Inorganic perovskite solar cells based on carbon electrodes. *Nano Energy* 77, 105160. doi:10.1016/j.nanoen.2020.105160

Wang, H. L., Yang, F., Li, X. H., and Zhang, P. T. (2024). Fully printed high-performance quasi-two-dimensional perovskite solar cells via multifunctional interfacial engineering. *Adv. Funct. Mater.* 34 (10). doi:10.1002/adfm.202312250

Wang, R., Xue, J., Meng, L., Lee, J. W., Zhao, Z., Sun, P., et al. (2019). Caffeine improves the performance and thermal stability of perovskite solar cells. *Joule* 3 (6), 1464–1477. doi:10.1016/j.joule.2019.04.005

Wang, W. R., Peng, X., Zhang, J., Lin, J., Huang, R., Zhang, G., et al. (2024). Dimethylamine oxalate manipulating CsPbI3 perovskite film crystallization process for high efficiency carbon electrode based perovskite solar cells. *J. Energy Chem.* 93, 221–228. doi:10.1016/j.jechem.2024.01.059

Wang, Y., Zhao, H., Mei, Y. M., Liu, H. L., Wang, S. R., and Li, X. G. (2019). Carbon nanotube bridging method for hole transport layer-free paintable carbon-based perovskite solar cells. *Acs Appl. Mater. and Interfaces* 11 (1), 916–923. doi:10.1021/acsami.8b18530

Wang, Y. D., Li, W., Yin, Y., Wang, M., Cai, W., Shi, Y., et al. (2022). Defective MWCNT enabled dual interface coupling for carbon-based perovskite solar cells with efficiency exceeding 22%. *Adv. Funct. Mater.* 32 (31), 2204831. doi:10.1002/adfm.202204831

Weerasinghe, H. C., Macadam, N., Kim, J. E., Sutherland, L. J., Angmo, D., Ng, L. W. T., et al. (2024). The first demonstration of entirely roll-to-roll fabricated perovskite solar cell modules under ambient room conditions. *Nat. Commun.* 15 (1), 1656. doi:10.1038/s41467-024-46016-1

Wu, X., Qi, F., Li, F., Deng, X., Li, Z., Wu, S., et al. (2021). Low-temperature processed carbon electrode-based inorganic perovskite solar cells with enhanced photovoltaic performance and stability. *Energy and Environ. Mater.* 4 (1), 95–102. doi:10.1002/eem2.12089

Wu, Z. F., Liu, Z., Hu, Z., Hawash, Z., Qiu, L., Jiang, Y., et al. (2019). Highly efficient and stable perovskite solar cells via modification of energy levels at the perovskite/carbon electrode interface. *Adv. Mater.* 31 (11), 1804284. doi:10.1002/adma.201804284

Xiang, J. W., Cheng, Y., Zhang, G., Liu, Z., Han, C., Gao, Q., et al. (2024). Efficient carbon-based hole-conductor-free printable mesoscopic perovskite solar cells via a multifunctional fluorinated molecule. *Adv. Funct. Mater.* 34. doi:10.1002/adfm.202402816

Xiao, J. W., Shi, C. B., Zhou, C. X., Zhang, D. L., Li, Y. J., and Chen, Q. (2017). Contact engineering: electrode materials for highly efficient and stable perovskite solar cells. *Sol. Rrl* 1 (9), 1700082. doi:10.1002/solr.201700082

Xiao, Y. Q., Zhang, H. J., Zhao, Y., Liu, P., Kondamareddy, K. K., and Wang, C. L. (2023). Carrier modulation via tunnel oxide passivating at buried perovskite interface for stable carbon-based solar cells. *Nanomaterials* 13 (19), 2640. doi:10.3390/nano13192640

Xie, P. F., Zhang, G., Yang, Z., Pan, Z., Fang, Y., Rao, H., et al. (2020). Perovskite-compatible carbon electrode improving the efficiency and stability of $CsPbI_2Br$ solar cells. *Sol. Rrl* 4 (11). 2000431. doi:10.1002/solr.202000431

Xu, D., Wang, D., Liu, J., Qi, J., Chen, K., Zhu, W., et al. (2024). Dual defect passivation at the buried interface for printable mesoscopic perovskite solar cells with reduced open-circuit voltage loss. *Small* 20, e2311755. doi:10.1002/smll.202311755

Xu, T. T., Wan, Z., Tang, H., Zhao, C., Lv, S., Chen, Y., et al. (2021). Carbon quantum dot additive engineering for efficient and stable carbon-based perovskite solar cells. *J. Alloys Compd.* 859, 157784. doi:10.1016/j.jallcom.2020.157784

Yang, F., Dong, L., Jang, D., Saparov, B., Tam, K. C., Zhang, K., et al. (2021). Low temperature processed fully printed efficient planar structure carbon electrode perovskite solar cells and modules. *Adv. Energy Mater.* 11 (28), 2101219. doi:10.1002/aenm.202101219

Ye, H. B., Liu, Z., Liu, X., Sun, B., Tan, X., Tu, Y., et al. (2019). 17.78% efficient low-temperature carbon-based planar perovskite solar cells using Zn-doped SnO_2 electron transport layer. *Appl. Surf. Sci.* 478, 417–425. doi:10.1016/j.apsusc.2019.01.237

Yu, Y. Y., Hoang, M. T., Yang, Y., and Wang, H. X. (2023). Critical assessment of carbon pastes for carbon electrode-based perovskite solar cells. *Carbon* 205, 270–293. doi:10.1016/j.carbon.2023.01.046

Yu, Y. Y., Yang, Y., Hoang, M. T., Chiu, W. H., Pang, L., O'Mullane, A. P., et al. (2024). Incorporation of liquid metal gallium into carbon electrode for efficient charge transportation in planar perovskite solar cells. *Sol. Rrl* 8 (1). doi:10.1002/solr.202300732

Yue, G. Q., Chen, D., Wang, P., Zhang, J., Hu, Z. Y., and Zhu, Y. J. (2016). Low-temperature prepared carbon electrodes for hole-conductor-free mesoscopic perovskite solar cells. *Electrochimica Acta* 218, 84–90. doi:10.1016/j.electacta.2016.09.112

Zhang, H. Y., Song, K. K., Zhu, L. Q., and Meng, Q. B. (2020). Back-interface regulation for carbon-based perovskite solar cells. *Carbon* 168, 372–391. doi:10.1016/j.carbon.2020.06.065

Zhang, H. Y., Xiao, J., Shi, J., Su, H., Luo, Y., Li, D., et al. (2018). Self-adhesive macroporous carbon electrodes for efficient and stable perovskite solar cells. *Adv. Funct. Mater.* 28 (39), 1802985. doi:10.1002/adfm.201802985

Zhang, J., Hu, X. G., Ji, K., Zhao, S., Liu, D., Li, B., et al. (2024a). High-performance bifacial perovskite solar cells enabled by single-walled carbon nanotubes. *Nat. Commun.* 15 (1), 2245. doi:10.1038/s41467-024-46620-1

Zhang, J., Cheng, N., Zhou, H., Zhong, J., He, F., Chen, Y., et al. (2024b). Dual-sites passivation for efficient and stable carbon-based perovskite solar cells. *Mater. Today Energy* 43, 101599. doi:10.1016/j.mtener.2024.101599

Zhang, X., Yu, Z. H., Zhang, D., Tai, Q. D., and Zhao, X. Z. (2023). Recent progress of carbon-based inorganic perovskite solar cells: from efficiency to stability. *Adv. Energy Mater.* 13 (33), 2201320. doi:10.1002/aenm.202201320

Zhang, Z. Y., Fan, W., Wei, X., Zhang, L., Yang, Z., Wei, Z., et al. (2019). Promoted performance of carbon based perovskite solar cells by environmentally friendly additives of CH_3COONH_4 and $Zn(CH_3COO)_2$. *J. Alloys Compd.* 802, 694–703. doi:10.1016/j.jallcom.2019.06.161

Zhao, W., Wu, L., Chen, J., Ju, J., Zeng, Y., Wu, Z., et al. (2024). Multifunctional interface modification enables efficient and stable HTL-free carbon-electroded $CsPbI_2Br$ perovskite solar cells. *Chemsuschem* 17. doi:10.1002/cssc.202400223

Zhu, S. S., Tian, J. Q., Zhang, J. J., Gao, C. X., and Liu, X. Z. (2021). Improving the interfacial contact of screen-printed carbon electrodes for perovskite solar cells. *Acs Appl. Energy Mater.* 4 (6), 5554–5559. doi:10.1021/acsaem.1c00232

Zou, L., Li, X., Yang, M., Yan, J., Wang, J., Cheng, J., et al. (2023). ZnPc/CsPbBr3 QDs collaborative interface modification to improve the performance of CsPbBr3 perovskite solar cells. *Sol. Energy Mater. Sol. Cells* 251, 112157. doi:10.1016/j.solmat.2022.112157

Zouhair, S., Clegg, C., Valitova, I., March, S., Jailani, J. M., and Pecunia, V. (2024). Carbon electrodes for perovskite photovoltaics: interfacial properties, meta-analysis, and prospects. *Sol. Rrl* 8 (6). doi:10.1002/solr.202300929